Ceramics International 45 (2019) 11304–11308

Contents lists available at ScienceDirect

Ceramics International

journal homepage: www.elsevier.com/locate/ceramint

Optical and electrical properties of (111)-oriented epitaxial $SrVO_3$ thin films

Ruixing Xu[a], Yanda Ji[a,**], Raouf Bouchilaoun[a], Fengjiao Qian[a], Min Li[a], Xiyuan Zhang[a], Rujun Tang[b], Run Zhao[c], Shikhar Misra[d], Haiyan Wang[d], Weiwei Li[e], Caixia Kan[a], Daning Shi[a], Jiyu Fan[a,***], Hao Yang[a,*]

[a] College of Science, Nanjing University of Aeronautics and Astronautics, Nanjing, 211106, China
[b] College of Physics, Optoelectronics and Energy, Soochow University, Suzhou, 215000, China
[c] College of Mathematics and Physics, Suzhou University of Science and Technology, Suzhou, 215000, China
[d] School of Materials Engineering, Electrical and Computer Engineering, Purdue University, West Lafayette, IN, 47907, USA
[e] Department of Materials Science and Metallurgy, University of Cambridge, 27 Charles Babbage Road, Cambridge, CB3 0FS, United Kingdom

ARTICLE INFO

Keywords:
TCO
$SrVO_3$
Strongly correlated oxide
(111)-oriented

ABSTRACT

Perovskite oxide $SrVO_3$ (SVO) is a transparent conductor with excellent optical and electrical properties. Most of the previous works have focused on (001)-oriented SVO thin films. As an alternative to tin-doped indium oxide (ITO), the other orientations of SVO thin films are important to be considered as well. In the present work, the optical and electrical properties of (111)-oriented SVO epitaxial films have been investigated. Excellent electrical conductivity (2.92×10^4 S cm^{-1}) and optical transparency (56.6%) have been demonstrated, which are comparable to those of ITO and expand the applications of epitaxial SVO thin films in other orientations as transparent conducting oxide.

1. Introduction

The study of transparent conducting thin films has attracted great interests due to the fast development and increasing demands for digital display technologies. Transparent conducting materials form a unique class of materials, which simultaneously possess high electrical conductivity and high optical transmission at visible frequencies. However, in most traditional materials, these two properties can hardly coexist [1,2]. Most materials with high conductivity usually have high carrier concentration and narrow band gap. However, the absorbable photon wavelength increases with the decreasing band gap and the higher the carrier concentration, the higher reflection. Nowadays, among few notable materials, tin-doped indium oxide (ITO) is regarded as the most successful transparent conductor. In optimally doped ITO (about 8% Sn doping in In_2O_3), the carrier concentration is in the order of 10^{21} cm^{-3}, slightly lower than a normal metal [3,4]. Meanwhile, it shows a high optical transparency which approaches 90% transmittance at the visible light frequencies. However, the shortage of indium limits the application of ITO, thus searching for a replacement of ITO is urgently required [5].

$SrVO_3$ (SVO) is regarded as one of the most promising candidates for transparent conducting oxides. It's a cubic perovskite (space group $Pm\bar{3}m$) and a simple paramagnetic metal with one electron in the 3*d* band, which attracts intensive researches for investigating the effects of electron correlation and testing the effectiveness of newly developed theoretical methods [6,7]. Besides, previous works also reported that (001)-oriented SVO thin films show metallic behaviors with a carrier concentration of around 2.2×10^{22} cm^{-3} at room temperature [8–10]. And SVO thin film grew on $(LaAlO_3)_{0.3}(Sr_2AlTaO_6)_{0.7}$ (LSAT) with a thickness of 45 nm possesses light transparency around 65% and a screened plasma frequency below 1.33eV [11]. These properties make SVO promising candidate for transparent conducting oxides. Besides, the high electrical conductivity and structural compatibility with other functional perovskites also makes it an excellent choice as bottom electrode.

Well known, by utilizing various substrates with different lattice parameters, one can manipulate the films' properties *via* the strain caused by the lattice mismatch between the substrate and the film [12–15]. In previous works, (001)-oriented substrates were mainly used, such as $SrTiO_3$ (STO), $LaAlO_3$ (LAO), and LSAT, *etc.* [16–18]. To the best of our knowledge, only few works reported the growth of SVO films with (110) and (111) orientations [8,16,19,20]. It has also been

* Corresponding author.
** Corresponding author.
*** Corresponding author.
E-mail addresses: jiyanda@nuaa.edu.cn (Y. Ji), jiyufan@nuaa.edu.cn (J. Fan), yanghao@nuaa.edu.cn (H. Yang).

https://doi.org/10.1016/j.ceramint.2019.02.207
Received 28 November 2018; Received in revised form 15 February 2019; Accepted 28 February 2019
Available online 05 March 2019
0272-8842/

demonstrated that the physical properties can be significantly changed by using different oriented substrates [21–24]. In addition, the different orientations of SVO films are needed in complex and changeable practical applications. Therefore, it is technically important and fundamental interesting to investigate the growth of SVO films with other directions and related properties. The high vacuum ($< 10^{-4}$ pa) was used in the most published studies. Highly hermetic equipment and more energy are required to maintain such a high vacuum. This seriously restricts the industrial application of SVO films. In this work, epitaxial (111)-oriented SVO thin films were fabricated on the (111)-oriented STO substrates under a high oxygen pressure (1×10^{-2} pa). The crystal structure has been revealed by combination of X-Ray Diffraction (XRD) and Transmission Electron Microscopy (TEM). Transport data confirms that SVO films show an excellent metallic behavior from 350 to 5 K with a carrier concentration in the order of 10^{22} cm^{-3} at room temperature. Moreover, a high optical transmission of 56.6% in the visible region has been found in a 40 nm film. Our work complements the absence of studies on SVO films with different orientations and expands the application scope of the SVO thin films.

2. Experimental details

Epitaxial (111)-oriented SVO thin films were grown on (111)-oriented STO substrates by Pulsed Laser Deposition (PLD). A sintered $SrVO_3$ ceramic target was focused by a pulsed excimer laser (Lambda Physik, 248 nm, 2 Hz, 3 J cm^{-2}). A substrate temperature of 630 °C and an oxygen pressure of 1×10^{-2} Pa were used. After deposition, the thin films were *ex-situ* post-annealed at 780 °C and 2 h under a flowing gas of 95 vol% Ar + 5 vol% H_2 for stabilizing the V valence states and relaxing growth-related strain [25–30]. Thin films with thicknesses of 40, 80 and 120 nm were fabricated. The crystal structure was investigated by XRD (Panalytical Empyrean) and TEM (FEI TALOS 200X operated at 200 kV). Transport properties and Hall coefficient were measured using the standard four-probe method in a Physical Properties Measurement System (PPMS-9, Quantum Design) in the temperature range of 350 to 5 K. Optical properties were investigated using SHIMADZU UV-3600plus within the 2500-300 nm wavelength range. The film thickness and surface morphology were determined by Atomic Force Microscopy (AFM, Asylum Research MFP-3D-SA). (001)-oriented SVO film has been fabricated on STO substrate with the same preparation process as that performed for (111)-oriented SVO film. The structural, optical and electrical properties of the (001)-oriented SVO films were provided in the supporting information (Fig S1, S2 and S3).

3. Results and discussion

3.1. Structural characterization

Fig. 1(a) presents a typical XRD θ-2θ spectrum for a 40 nm thick SVO film, which only has (111) peaks derived from the SVO film and STO substrate. An inter-planar spacing of SVO along the (111) orientation is calculated to be 2.218 ± 0.003 Å, consistence with bulk lattice parameters. Fig. 1(b) shows phi scans (φ-scans) spectrum measured from (011) planes of STO substrate and SVO film, revealing an epitaxial nature of $(111)_{SVO}//(111)_{STO}$ and $[011]_{SVO}//[011]_{STO}$ (shown as Fig. 1(c)). As shown in Fig. 1(d), the Reciprocal Space Map (RSM) around the (033) peak of STO substrate and SVO film was measured and confirms that the growth-related strain is fully relaxed. The SVO film presents a very smooth morphology with a Root Mean Square (RMS) roughness of around 0.3 nm (Fig. S4(a), Supporting information).

To further investigate the microstructure of SVO film, TEM and scanning transmission electron microscopy (STEM) analyses were conducted. Fig. 2(a) shows the cross-section STEM image taken under high angle annular dark field (HAADF) condition where the image contrast is roughly proportional to Z^2. Clearly, the uniform contrast confirms the single phase growth of the SVO film. The Energy Dispersive Spectrometer (EDS) elemental map of V and Ti presented in Fig. 2(b) shows a clear boundary between V element and Ti element suggesting no obvious inter-diffusion with the substrate. The fast Fourier transformation (FFT) patterns, using the selected area high-resolution TEM data (square area), reveals the growth direction of the film as $(111)_{SVO}//(111)_{STO}$ and $[011]_{SVO}//[011]_{STO}$ (shown as Fig. 2(c)). These results are consistent with the XRD results in Fig. 1(a).

3.2. Electrical transport properties

The electrical transport properties of perovskite-type SVO are always emphasized because of its special band structures [31]. Recent results show that a transition from metal to insulator occurs with a reduced film thickness (such as 6.5 nm), which contributed to the variation of dimension [32,33]. The film/substrate exchange and induced strains also affects the conductivity of SVO films [34,35]. In order to achieve intrinsic properties of SVO thin film, here, we mainly focus on thicker SVO films with thickness beyond 40 nm to mitigate the strain effects and lattice mismatch of STO substrate. We selected three different SVO thin films with thicknesses of 40, 80 and 120 nm in the present work. Fig. 3(a) shows the temperature-dependent resistivity in the temperature range from 350 to 5 K. All samples show metallic behaviors at the measured temperature range. The room-temperature resistivities are 3.91×10^{-5}, 3.42×10^{-5}, and 3.21×10^{-5} Ω cm for 40, 80 and 120 nm thick films, respectively. Corresponded electrical conductivities are determined to be 2.56×10^{4}, 2.92×10^{4}, and 3.12×10^{4} S cm^{-1}. These values are comparable to those of the (001)-oriented SVO films (shown in Fig. S2). The inset of Fig. 3(a) shows the measured Hall effect in an 80 nm thick SVO film. The carrier concentration and mobility are deduced to be 2.61×10^{22} cm^{-3} and 7.01 cm^2 V^{-1} s^{-1} respectively, which are similar to those of the (001)-oriented SVO film. Similar Hall effect results have also been found in the 40 and 120 nm thick films (not shown) and all the calculated parameters are listed in Table 1. Obviously, metallic behavior was retained for the SVO films with (111) orientation.

To understand the physical mechanism underlying the metallic behavior, we use the simple electron-electron interaction model to fit the experimental results. The fitting formula is expressed by $\rho = \rho_0 + AT^2$ [19], where ρ_0 and A are the residual resistivity and a coefficient correlated with the electron-electron interactions, respectively. As shown in Fig. 3(b), the fitting curve is overlapped well with the experimental result for the 40 nm thick film, indicating that the electron-electron interaction is mainly responsible for the resistivity in the SVO film. Another two fitting results for 80 and 120 nm thick films have also been obtained and were listed in Table 1. It is well known that the value of A quantifies the electron-electron interactions in the strongly correlated system.

3.3. Optical transmission properties

The optical transmittance of SVO films across the wavelength range of 2500-300 nm are shown in Fig. 4. Photographs of samples on a colored background are also shown as the insets. The transmittance of all SVO films increases with the decreasing wavelength and reaches a maximum at around 550 nm, and then it drops sharply to 0%. The intense decrease in the transmittance at the wavelength near 400 nm originated from a STO intra-band transition located at around 3.2 eV. The maximum transmittance of a 40 nm thick film is around 56.6%, which is comparable to that of the (001) SVO (56.3% shown in Fig. S3) and indicates that the (111) oriented SVO films also show good transparency [9–11].

4. Conclusions

In summary, the (111)-oriented SVO thin films were fabricated on

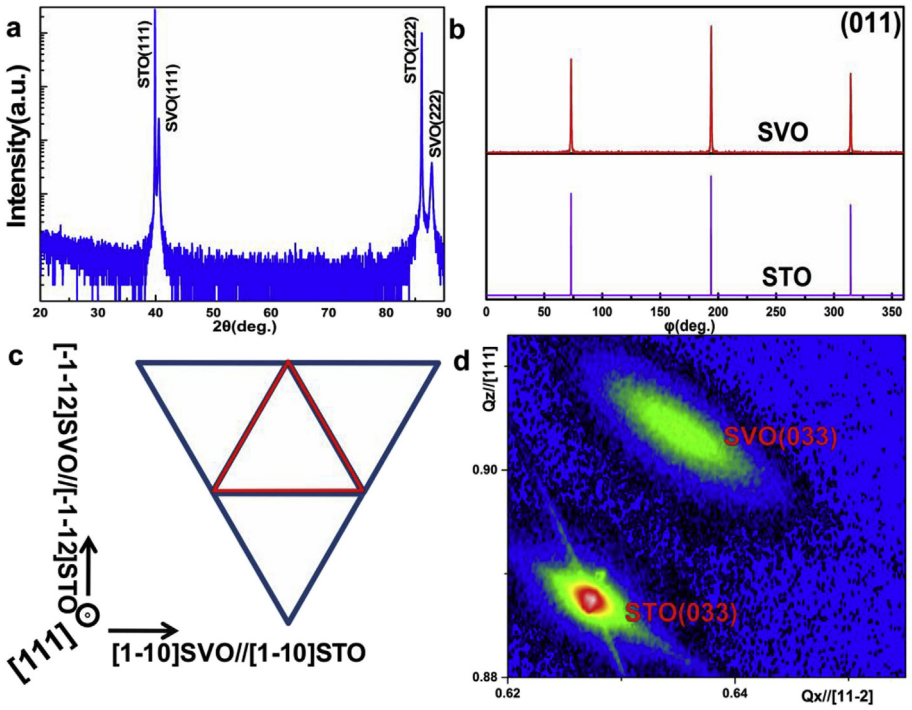

Fig. 1. a) X-Ray Diffraction spectra ($\theta-2\theta$ scan). B) 360° ϕ-scan of the (011) reflection of the SVO thin film (top panel) and the STO substrate (bottom panel). c) The in-plane arrangements of monoclinic SVO unit cells on (111) STO substrate d) Reciprocal space maps along the (033) STO reflection.

STO substrates by PLD. An epitaxial nature of $(111)_{SVO}//(111)_{STO}$ and $[011]_{SVO}//[011]_{STO}$ has been revealed by the combination of XRD and TEM. The measurements of transport behaviors show that SVO films keep an excellent metallic behavior from 350 to 5 K with a carrier concentration in the order of 10^{22} cm^{-3} at room temperature. And a high optical transmission of 56.6% has been found in a 40 nm thick film. This work shows that SVO films with different orientations are potential and feasible TCOs for the future.

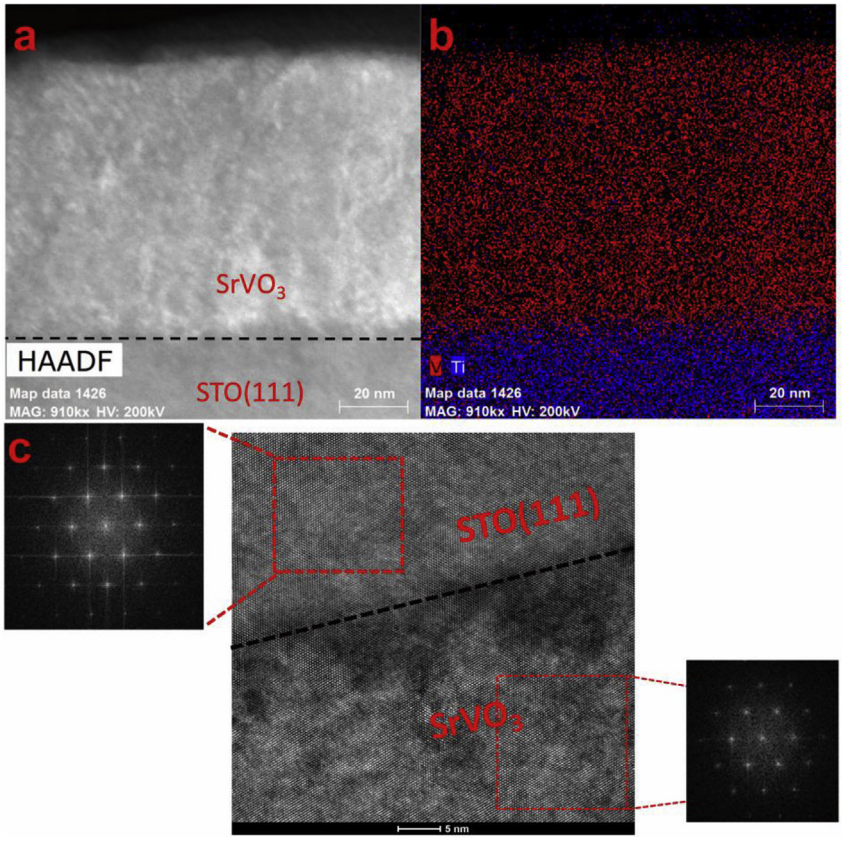

Fig. 2. TEM and STEM images of the SVO film on (111)-oriented STO substrate; **a** HAADF-STEM image; **b** Energy dispersive spectroscopy (EDX) map of the corresponding area in a; **c** High-resolution TEM (HRTEM) image at the interface of SVO on STO (111) and the corresponding fast Fourier transform (FFT) patterns of the film and substrate areas indicating the high quality epitaxial growth of the SVO film.

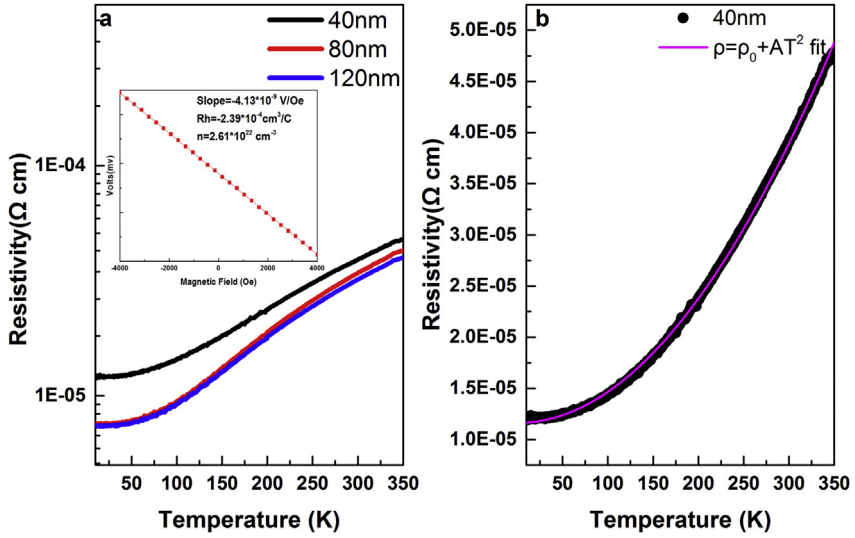

Fig. 3. a Temperature-dependent resistivity of SVO thin films with thicknesses of 40, 80 and 120 nm. The inset shows the Hall effect measurement of a 80 nm thick film; **b** Electrical resistivity vs. Temperature for a 40 nm thick SVO film. The solid line represents the fitting data with a formula of $\rho = \rho_0 + AT^2$.

Table 1
Calculated parameters of SVO films with various thicknesses.

Sample	40 nm	80 nm	120 nm
Carrier concentration, n (cm^{-3})	2.13×10^{22}	2.61×10^{22}	2.23×10^{22}
Residual resistivity, ρ_0 (Ω·cm)	1.16×10^{-5}	6.86×10^{-6}	6.82×10^{-6}
Coefficient correlated with the electron-electron interactions, A (Ω·cm·K^{-2})	3.04×10^{-10}	3.01×10^{-10}	2.77×10^{-10}
Maximum Transmission, T (%)	56.6	51.6	34.7
Mobility, μ(cm^2·V^{-1}·s^{-1})	7.51	7.01	8.74

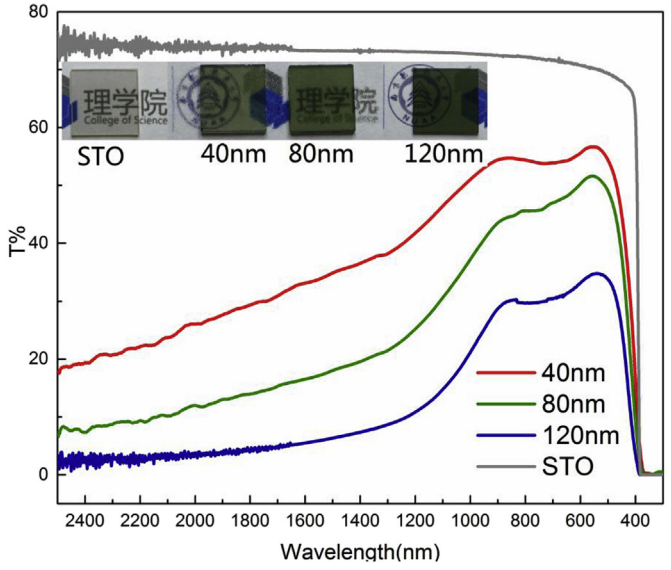

Fig. 4. Transmission spectrum of SVO films with varying thickness on STO substrates. The inset show photographs of SVO thin films on STO and bare STO substrate.

Acknowledgments

This work was supported by the National Nature Science Foundation of China (Grant No. U1632122, 11774172, 11774171, 11874220, 51772200, 51602152, and 11704272), the Fundamental Research Funds for the Central Universities (Grant No. NE2016102 and NP2017103), and the Nature Science Foundation of Jiangsu Province (No. BK20180418). H. W. and S. M. acknowledge the support from the U.S. National Science Foundation (DMR-1809520) for the effort at Purdue University. W. L. acknowledges the support from EPSRC grant EP/L011700/1, EP/N004272/1, and the Isaac Newton Trust (Minute 13.38(k)).

Appendix A. Supplementary data

Supplementary data to this article can be found online at https://doi.org/10.1016/j.ceramint.2019.02.207.

References

[1] J.R. Bellingham, W. A.P., C.J. Adkins, Intrinsic performance limits in transparent conducting oxides, J. Mater. Sci. Lett. 11 (5) (1992) 263–265.
[2] T.J. Coutts, D.L. Young, X. Li, Characterization of transparent conducting oxides, MRS Bull. 25 (08) (2011) 58–65.
[3] J. Lewis, et al., Highly flexible transparent electrodes for organic light-emitting diode-based displays, Appl. Phys. Lett. 85 (16) (2004) 3450–3452.
[4] S.-I. Na, et al., Efficient and flexible ITO-free organic solar cells using highly conductive polymer anodes, Adv. Mater. 20 (21) (2008) 4061–4067.
[5] K. Ellmer, Past achievements and future challenges in the development of optically transparent electrodes, Nat. Photon. 6 (12) (2012) 809–817.
[6] A. Georges, et al., Dynamical mean-field theory of strongly correlated fermion systems and the limit of infinite dimensions, Rev. Mod. Phys. 68 (1) (1996) 13–126.
[7] G. Kotliar, et al., Electronic structure calculations with dynamical mean-field theory, Rev. Mod. Phys. 78 (3) (2006) 865–951.
[8] B. Bérini, et al., Control of high quality SrVO3Electrode in oxidizing atmosphere, Adv. Mater. Interfaces 3 (18) (2016) 1600274.
[9] A. Boileau, et al., Optical and electrical properties of the transparent conductor SrVO3 without long-range crystalline order, Appl. Phys. Lett. 112 (2) (2018) 021905.
[10] J.A. Moyer, C. Eaton, R. Engel-Herbert, Highly Conductive SrVO3 as a bottom electrode for functional perovskite oxides, Adv. Mater. 25 (26) (2013) 3578–3582.
[11] L. Zhang, et al., Correlated metals as transparent conductors, Nat. Mater. 15 (2) (2015) 204–210.
[12] C. Ma, et al., Anisotropic strain induced directional metallicity in highly epitaxial LaBaCo2O5.5+delta thin films on (110) NdGaO3, Sci. Rep. 6 (2016) 37337.
[13] H. Yang, et al., Vertical interface effect on the physical properties of self-assembled nanocomposite epitaxial films, Adv. Mater. 21 (37) (2009) 3794–3798.
[14] K. Jiang, et al., Strain and temperature dependent absorption spectra studies for identifying the phase structure and band gap of EuTiO3 perovskite films, Phys. Chem. Chem. Phys. 17 (47) (2015) 31618–31623.
[15] X.Z. Lu, J.M. Rondinelli, Epitaxial-strain-induced polar-to-nonpolar transitions in layered oxides, Nat. Mater. 15 (9) (2016) 951–955.
[16] M. Chi, et al., Atomic and electronic structures of the SrVO3-LaAlO3 interface, J. Appl. Phys. 110 (4) (2011) 046104.
[17] A. Fouchet, et al., Study of the electronic phase transition with low dimensionality in SrVO3 thin films, Mater. Sci. Eng. B 212 (2016) 7–13.
[18] Y. Okada, et al., Quasiparticle interference on cubic perovskite oxide surfaces, Phys. Rev. Lett. 119 (8) (2017) 086801.

[19] M. Gu, S.A. Wolf, J. Lu, Two-Dimensional mott insulators in SrVO3Ultrathin films, Adv. Mater. Interfaces 1 (7) (2014) 1300126.
[20] J. Li, et al., Interfacial defects induced electronic property transformation at perovskite SrVO3/SrTiO3 and LaCrO3/SrTiO3 heterointerfaces, Phys. Chem. Chem. Phys. 19 (10) (2017) 6945–6951.
[21] S. Thiel, et al., Tunable quasi–two-dimensional electron gases in oxide heterostructures, Science 313 (2006) 1942–1945.
[22] Y.-L. Han, et al., Two-dimensional superconductivity at (110) LaAlO3/SrTiO3 interfaces, Appl. Phys. Lett. 105 (19) (2014) 192603.
[23] L. Yan, et al., Effects of crystallographic orientation on the oxygen exchange rate of La0.7Sr0.3MnO3 thin films, Solid State Ionics 194 (1) (2011) 9–16.
[24] M. Yan, et al., Electron channeling contrast imaging of anti-phase boundaries in coherently strained La0.7Sr0.3MnO3 thin films on (110)-oriented SrTiO3, Appl. Phys. Lett. 107 (4) (2015) 041601.
[25] R. Zhao, et al., Conduction mechanisms of epitaxial EuTiO3 thin films, Appl. Phys. Lett. 101 (10) (2012) 102901.
[26] K. Fujita, et al., High-quality antiferromagnetic $EuTiO_3$ epitaxial thin films on $SrTiO_3$ prepared by pulsed laser deposition and postannealing, Appl. Phys. Lett. 94 (6) (2009) 062512.
[27] J.H. Lee, et al., Optical band gap and magnetic properties of unstrained $EuTiO_3$ films, Appl. Phys. Lett. 94 (21) (2009) 212509.
[28] K.S. Takahashi, Control of the anomalous Hall effect by doping in Eu1 − xLaxTiO3Thin films, Phys. Rev. Lett. 103 (5) (2009) 057204.
[29] G.T. Gibson, et al., Oxygen depth profiling by nuclear resonant scattering, AIP Conf. Proc. 475 (1) (1999) 549.
[30] Luke S.-J. Peng, et al., Strain relaxation during in situ growth of $SrTiO_3$ thin films, Appl. Phys. Lett. 83 (22) (2003) 4592.
[31] P. Dougier, J.C. C.F, J.B. Goodenough, Etude des Proprietes Magnetiques, Electriques et Optiques des Phases de Structure Perovskite SrV02.90 et SrVO3, J. Solid State Chem. 14 (3) (1975) 247–259.
[32] Q.R. Li, et al., Dimensional crossover in ultrathin buried conducting SrVO3 layers, Phys. Rev. B 91 (3) (2015).
[33] Z. Zhong, et al., Electronics with correlated oxides: SrVO(3)/SrTiO(3) as a mott transistor, Phys. Rev. Lett. 114 (24) (2015) 246401.
[34] Kubicek Markus, et al., Tensile lattice strain accelerates oxygen surface exchange and diffusion in La1-xSrxCoO3-δThin films, ACS Nano 7 (4) (2013) 3276.
[35] R.Petrie Jonathan, et al., Strain control of oxygen vacancies in epitaxial strontuim cobaltite films, Adv. Funct. Mater. 26 (10) (2016) 1564–1570.